Available online at www.sciencedirect.com
SCIENCE DIRECT®
Journal of Sound and Vibration 269 (2004) 251–271
JOURNAL OF SOUND AND VIBRATION
www.elsevier.com/locate/jsvi

Three-dimensional steady state Green function for a layered isotropic plate

H. Bai[a], J. Zhu[b], A.H. Shah[a,*], N. Popplewell[a]

[a] *Department of Civil Engineering, Faculty of Engineering, University of Manitoba, Winnipeg, Man., Canada R3T 5V6*
[b] *Integrated Engineering Software, Winnipeg, Man., Canada R3H 0X4*

Received 14 February 2002; accepted 14 December 2002

Abstract

The elastodynamic response of a layered isotropic plate to a source point load having an arbitrary direction is studied in this paper. A decomposition technique is developed within each homogeneous isotropic lamina to simplify the general three-dimensional plane-wave propagation problem as a separate plane-strain problem and an anti-plane-wave propagation problem. The accuracy of computation is assured by cross-checking the numerical results by different methods. Results are checked numerically for a vertical point load acting on a homogeneous and a layered plate by using a hybrid method. On the other hand, results are checked for a horizontal point load by using dynamic reciprocal identities. Results are presented for both a homogeneous as well as a layered plate.

1. Introduction

Wave propagation in an infinite, elastic plate has been studied since the last century. Practical applications include the ultrasonic non-destructive evaluation of defects and the characterization of a material's properties. Two different approaches have been generally employed. One is a wave spectra analysis based on the frequency equation and the other involves fundamental elastodynamic solutions arising from the Green function which correspond to a structure's dynamic responses to a source load. It is envisioned that a Green function is essential for applying the boundary element method (BEM) to study the effects of cracks and other flaws in a plate.

The elastodynamic Green function for a homogeneous isotropic plate has been investigated for many years. See, for example, the comprehensive literature review by Miklowitz [1]. Most

*Corresponding author. Tel.: +204-474-9441; fax: +204-474-7513.
E-mail address: shah@cc.umanitoba.ca (A.H. Shah).

0022-460X/03/$ - see front matter
doi:10.1016/S0022-460X(03)00071-3

previous studies deal with two-dimensional problems (i.e., the plane-strain or plane-stress cases). Weaver and Pao [2], for instance, studied the dynamic response of an isotropic plate to a vertical load in which axisymmetry holds. Fundamental three-dimensional transient solutions, on the other hand, have been developed by Ceranoglu and Pao [3]. Their analysis is based on a generalized ray theory and Cagniard's method. The latter is used to invert the double transform arising in the solution. In the generalized ray method, however, only a finite number of rays are presumed to be important at some finite instant. However, many rays have to be considered in practice so that numerical calculations are tedious for late instants. The transient solution to an embedded dislocation can be found in Vasudevan and Mal [4]. They employed an integral transform technique.

The dynamic response due to a source load in an anisotropic plate has also been reported in the literature. For example, two-dimensional transient wave propagation in an anisotropic plate caused by a line load was studied by Scott and Miklowitz [5,6] as well as by Willis and Bedding [7]. Green and Green [8] and Green [9,10] investigated the transient stresses in a four-ply fiber-composite plate for both inextensible and extensible fibers. Their solution was based on the contributions of solely the propagating modes. Liu et al. [11] proposed a hybrid numerical method to compute the transient waves propagating in a laminated anisotropic plate from a short duration line load and a vertical point load. The displacement response was determined by employing a Fourier transform and modal analysis. However, only 10 modes were considered in their computation. Zhu et al. [12] and Zhu and Shah [13] presented a modal representation of the plane-strain, elastodynamic Green function for laminated composite plates. Contributions from all the modes gave accurate results in both the near and far fields. Recently, the axisymmetric transient dynamic response in a transversely isotropic plate was found by Weaver et al. [14]. In a fundamental three, rather than two-dimensional solution, Mal and Lih [15] as well as Xu and Mal [16,17] employed a wave number integral approach to find the elastodynamic response of a unidirectional composite plate to a vertical point load or a line load. However, the wave number integral requires complex integration. To the authors' knowledge, no efficient numerical method has been derived to compute the three-dimensional Green function.

Attention is devoted in this paper to a modal representation of the three-dimensional, elastodynamic Green function in a layered isotropic plate due to a source point load which may be oriented arbitrarily. The plate is composed of perfectly bonded lamina, each of which has a distinct thickness as well as isotropic material properties. For each isotropic lamina, the three-dimensional, plane-wave propagation problem is decomposed into a plane-strain problem in addition to a separate anti-plane problem. The complexities of an arbitrarily laminated profile are circumvented for the layered plate by employing finite element modelling in the thickness direction (Dong and Huang [18]) to determine the wave modes. For a plane-wave, the wave modes are obtained by using eigendata extracted from two independent algebraic eigensystems; one for the plane-strain problem and the other for the anti-plane problem. Explicit forms of the Green function are constructed by first summing the wave modes of a plane-wave and then superposing the plane-wave solutions in the circumferential direction. The procedure detailed here will be designated as a plane-wave superposition technique. A similar procedure can also be used to construct the Green function for laminated composite plates.

As a cross check, the axisymmetric Green function of a homogeneous as well as layered plate excited by a vertical point load is derived by using a hybrid model. In the hybrid model, a finite

element representation is employed in the vicinity of the point load (i.e., in the interior region) whilst a wave function expansion is used in the exterior region. It is shown that the numerical results from the proposed method and the hybrid method are in very good agreement. The hybrid method presented here cannot be applied to the case of a horizontal point load since axisymmetry does not hold. However, a cross check is performed by considering the dynamic reciprocal relation. The numerical results are in excellent agreement.

2. Formulation

The time-harmonic elastic wave propagation in an infinite, laminated isotropic plate is considered next. The laminated plate has perfectly bonded isotropic laminas that are separate entities, each enjoying distinct mechanical properties and thicknesses. The two outer surfaces of the plate are considered to be traction free with a separation of $2H$. Assume that the waves travel in the x' direction, which has an angle ϕ to the x direction of the global (x, y, z) co-ordinate system shown in Fig. 1. The three-dimensional, time-harmonic wave motion equation for each isotropic lamina can be written in the frequency domain as

$$\mu\nabla^2\mathbf{u} + (\lambda + \mu)\nabla(\nabla \bullet \mathbf{u}) + \rho\omega^2\mathbf{u} + \mathbf{b} = 0, \tag{1}$$

where λ and μ are Lame's constants, ρ is the mass density and ω is the circular frequency. Moreover,

$$\nabla = \left(\frac{\partial}{\partial x}, \frac{\partial}{\partial y}, \frac{\partial}{\partial z}\right)^{\mathrm{T}}, \quad \nabla^2 = \frac{\partial^2}{\partial x^2} + \frac{\partial^2}{\partial y^2} + \frac{\partial^2}{\partial z^2}, \tag{2}$$

and

$$\mathbf{u} = (u, v, w)^{\mathrm{T}}, \quad \mathbf{b} = \left(b_x, b_y, b_z\right)^{\mathrm{T}}, \tag{3}$$

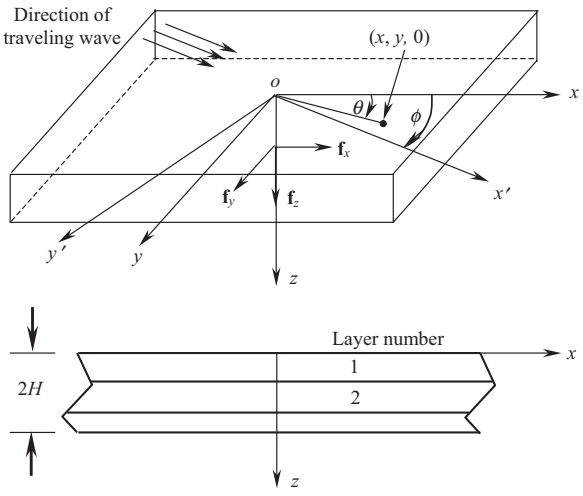

Fig. 1. Plate configuration.

where u, v, and w represent the displacements whilst b_x, b_y, and b_z correspond to the body forces in the x, y and z directions, respectively.

2.1. Construction of 3-D Green function

This section presents a modal representation of the three-dimensional time-harmonic Green function due to an arbitrarily oriented load in a layered isotropic plate.

2.1.1. Discrete equations of motion

A semi-analytical finite element method is used to formulate the governing equations. With this method, the x and y dependencies of $\mathbf{u}$ are accommodated by means of an analytical double integral Fourier transform, with the z dependence approximated by using finite elements. Then, by employing a proper co-ordinate transformation, the three-dimensional problem can be decomposed into a plane-strain problem and an anti-plane problem in the direction of the travelling waves. The Fourier transform employs transform pairs that are defined in terms of the wave numbers in the x and y directions, k_x and k_y, respectively, i.e.,

$$\tilde{f}(k_x, k_y, z) = \int_{-\infty}^{\infty}\int_{-\infty}^{\infty} f(x, y, z)\mathrm{e}^{-\mathrm{i}(k_x x + k_y y)}\mathrm{d}x\,\mathrm{d}y, \tag{4}$$

and

$$f(x, y, z) = \frac{1}{(2\pi)^2}\int_{-\infty}^{\infty}\int_{-\infty}^{\infty} \tilde{f}(k_x, k_y, z)\mathrm{e}^{\mathrm{i}(k_x x + k_y y)}\mathrm{d}k_x\,\mathrm{d}k_y, \tag{5}$$

where $\mathrm{i} = \sqrt{-1}$. Next, define k as a wave number in the x' direction which is oriented at angle ϕ to the x axis (see Fig. 1). Then the wave numbers k_x and k_y in the x and y directions, respectively, are given by

$$k_x = k\cos\phi \quad \text{and} \quad k_y = k\sin\phi. \tag{6}$$

After applying the Fourier transform (4) to Eq. (1) and making the co-ordinate transform from the (x, y, z) to the (x', y', z) co-ordinates, Eq. (1) can be rewritten as

$$\mu\frac{\mathrm{d}^2\tilde{u}'}{\mathrm{d}z^2} - (\lambda + 2\mu)k^2\tilde{u}' + \mathrm{i}(\lambda + \mu)k\frac{\mathrm{d}\tilde{w}'}{\mathrm{d}z} + \rho\omega^2\tilde{u}' + \tilde{b}'_{x'} = 0, \tag{7}$$

$$(\lambda + 2\mu)\frac{\mathrm{d}^2\tilde{w}'}{\mathrm{d}z^2} - \mu k^2\tilde{w}' + \mathrm{i}(\lambda + \mu)k\frac{\mathrm{d}\tilde{u}'}{\mathrm{d}z} + \rho\omega^2\tilde{w}' + \tilde{b}'_z = 0, \tag{8}$$

$$\mu\frac{\mathrm{d}^2\tilde{v}'}{\mathrm{d}z^2} - \mu k^2\tilde{v}' + \rho\omega^2\tilde{v}' + \tilde{b}'_{y'} = 0. \tag{9}$$

Here the prime quantities are referenced to the (x', y', z) co-ordinates. Eqs. (7) and (8) describe a plane-strain problem in the $x' - z$ plane. Eq. (9), on the other hand, represents an independent anti-plane problem in which waves travel in the x' direction. Consequently, the three-dimensional wave propagation problem in isotropic plates is decomposed into separate plane-strain and anti-plane problems. This decomposition is important because a complicated three-dimensional problem is solved by merely superimposing the solutions of two simpler problems having lower dimensions. Moreover, the plane-strain wave propagation problem has been investigated already

by efficiently using two-dimensional elastodynamic Green functions in a modal representation [12,19].

To solve the plane-strain and anti-plane problems that are defined by Eqs. (7)–(9), the z-dependence is found by using the finite element modelling detailed by Dong and Huang [18] (but not reproduced here). The approach starts by discretizing each lamina into several sublayers so that the total number of sublayers over the plate's thickness, $2H$, is N. The displacement distributions through the thickness of each sublayer are approximated by employing quadratic functions of a (variable) thickness. The generalized co-ordinates correspond to the nodal displacements at the top, middle and bottom surfaces of each sublayer. Thus, the total number of nodes through the thickness of the plate is $(2N+1)$. Then, by using a conventional finite element procedure, the discretized governing equations over the complete thickness profile of the plate can be derived for the plane-strain and anti-plane problems as

$$(k_p^2\mathbf{K}_{p1} - \mathrm{i}k_p\mathbf{K}_{p2} + \mathbf{K}_{p3} - \omega^2\mathbf{M}_p)\tilde{\mathbf{Q}}_p = \tilde{\mathbf{F}}_{x'z}, \tag{10}$$

and

$$(k_a^2\mathbf{K}_{a1} + \mathbf{K}_{a3} - \omega^2 M_a)\tilde{\mathbf{Q}}_a = \tilde{\mathbf{F}}_{y'}. \tag{11}$$

Subscripts p and a indicate the plane-strain and anti-plane problems, respectively. $\mathbf{K}_{pi}$, $\mathbf{K}_{ai}$, $\mathbf{M}_p$ and $\mathbf{M}_a$ are the corresponding assembled global stiffness and mass matrices for all the lamina. On the other hand, $\tilde{\mathbf{Q}}_p = (\tilde{\mathbf{U}}'^{\mathrm{T}}, \tilde{\mathbf{W}}'^{\mathrm{T}})^{\mathrm{T}}$ and $\tilde{\mathbf{Q}}_a = \tilde{\mathbf{V}}'$, as well as $\tilde{\mathbf{F}}_{x'z}$ and $\tilde{\mathbf{F}}_{y'}$ represent the total (global) nodal displacement and traction vectors in the transformed domain, respectively. The size of each stiffness and mass matrices is $M_p \times M_p$ for the plane-strain problem and $M_a \times M_a$ for the anti-plane problem. Consequently, the size of the nodal displacement and traction vectors is M_p for the plane-strain problem and M_a for the anti-plane problem where $M_p = 2(2N+1)$ and $M_a = 2N+1$. Note that $\mathbf{K}_{p1}$, $\mathbf{K}_{p3}$, $\mathbf{K}_{a1}$, $\mathbf{K}_{a3}$, $\mathbf{M}_p$ and $\mathbf{M}_a$ are symmetric but $\mathbf{K}_{p2}$ is antisymmetric.

2.1.2. *Eigenvalue problems and modal summations*

The first step in solving Eqs. (10) and (11) is to consider the homogeneous equations, which have the form of a two-parameter, algebraic eigensystem corresponding to the parameters ω and k_p or k_a. The k_p or k_a is adopted as the eigenvalue parameter when specific values are assigned, as here, to ω. The quadratic eigenproblems, corresponding to Eq. (10) for k_p and Eq. (11) for k_a, can be recast into the first order form

$$\left[\mathbf{A}_p(\omega) - k_p\mathbf{B}_p\right]\tilde{D}_p = \tilde{P}_p \ \text{ and } \ [\mathbf{A}_a(\omega) - k_a\mathbf{B}_a]\tilde{\mathbf{D}}_a = \tilde{\mathbf{P}}_a, \tag{12}$$

where

$$\mathbf{A}_p(\omega) = \begin{bmatrix} 0 & \mathbf{I} \\ \mathbf{K}_{p3} - \omega^2\mathbf{M}_p & -\mathrm{i}\mathbf{K}_{p2} \end{bmatrix}, \quad \mathbf{B}_p = \begin{bmatrix} \mathbf{I} & 0 \\ 0 & -\mathbf{K}_{p1} \end{bmatrix},$$
$$\mathbf{A}_a(\omega) = \begin{bmatrix} 0 & \mathbf{I} \\ \mathbf{K}_{a3} - \omega^2\mathbf{M}_a & 0 \end{bmatrix}, \quad \mathbf{B}_a = \begin{bmatrix} \mathbf{I} & 0 \\ 0 & -\mathbf{K}_{a1} \end{bmatrix}, \tag{13}$$

$$\tilde{\mathbf{D}}_p = (\tilde{\mathbf{Q}}_p^{\mathrm{T}}, k_p\tilde{\mathbf{Q}}_p^{\mathrm{T}})^{\mathrm{T}}, \quad \tilde{\mathbf{P}}_p = (0 \quad \tilde{F}_{x'z}^{\mathrm{T}})^{\mathrm{T}},$$
$$\tilde{\mathbf{D}}_a = (\tilde{\mathbf{Q}}_a^{\mathrm{T}}, k_a\tilde{\mathbf{Q}}_a^{\mathrm{T}})^{\mathrm{T}}, \quad \tilde{P}_a = (0 \quad \tilde{\mathbf{F}}_{y'}^{\mathrm{T}})^{\mathrm{T}}, \tag{14}$$

and $\mathbf{I}$ is an identity matrix.

Note that the linear transformations of Eqs. (10)–(12) double the dimensions of the displacement vectors in both problems. By setting $\tilde{\mathbf{P}}_p = 0$ and $\tilde{\mathbf{P}}_a = 0$, two sets of general eigenvalue problems are obtained in terms of the eigenvalues (denoted as k_{pm} and k_{am}), the associated left eigenvectors, ϕ_{pm}^L and ϕ_{am}^L, and the right eigenvectors, ϕ_{pm}^R and ϕ_{am}^R. The resulting two linear eigenvalue problems become

$$[\mathbf{A}_p(\omega) - k_{pm}\mathbf{B}_p]\phi_{pm}^R = 0, \quad [\mathbf{A}_p^{\mathrm{T}}(\omega) - k_{pm}\mathbf{B}_p^{\mathrm{T}}]\phi_{pm}^L = 0,$$
$$[\mathbf{A}_a(\omega) - k_{am}\mathbf{B}_a]\phi_{am}^R = 0, \quad \left[\mathbf{A}_a^{\mathrm{T}}(\omega) - k_{am}\mathbf{B}_a^{\mathrm{T}}\right]\phi_{am}^L = 0. \tag{15}$$

According to Eq. (14), the right and left eigenvectors can be partitioned into upper and lower halves as

$$\phi_{pm}^R = \begin{Bmatrix} \phi_{pmu}^R \\ \phi_{pml}^R \end{Bmatrix} = \begin{Bmatrix} \tilde{\mathbf{Q}}_{pm}^R \\ k_{pm}\tilde{\mathbf{Q}}_{pm}^R \end{Bmatrix}, \quad \phi_{pm}^L = \begin{Bmatrix} \phi_{pmu}^L \\ \phi_{pml}^L \end{Bmatrix} = \begin{Bmatrix} \tilde{\mathbf{Q}}_{pm}^L \\ k_{pm}\tilde{\mathbf{Q}}_{pm}^L \end{Bmatrix},$$
$$\phi_{am}^R = \begin{Bmatrix} \phi_{amu}^R \\ \phi_{aml}^R \end{Bmatrix} = \begin{Bmatrix} \tilde{\mathbf{Q}}_{am}^R \\ k_{am}\tilde{\mathbf{Q}}_{am}^R \end{Bmatrix}, \quad \phi_{am}^L = \begin{Bmatrix} \phi_{amu}^L \\ \phi_{aml}^L \end{Bmatrix} = \begin{Bmatrix} \tilde{\mathbf{Q}}_{am}^L \\ k_{am}\tilde{\mathbf{Q}}_{am}^L \end{Bmatrix}. \tag{16}$$

It may be noted that, for a particular value of ω, Eq. (15) will have both real and complex roots for k_p or k_a. The real (complex) roots correspond to propagating (evanescent) modes.

By following the modal summation technique of Liu et al. [11], as well as Liu and Achenbach [20], and applying the orthogonality conditions of the left and right eigenvectors, the displacement vectors for the plane-strain and anti-plane problems in the transformed domain, $\tilde{\mathbf{Q}}_p = (\tilde{\mathbf{U}}'^{\mathrm{T}}, \tilde{\mathbf{W}}'^{\mathrm{T}})^{\mathrm{T}}$ and $\tilde{\mathbf{Q}}_a = \tilde{\mathbf{V}}'$, are constructed as

$$\begin{Bmatrix} \tilde{\mathbf{U}}' \\ \tilde{\mathbf{W}}' \end{Bmatrix} = \sum_{m=1}^{2M_p} \frac{(\phi_{pml}^L)^{\mathrm{T}}\tilde{\mathbf{F}}_{x'z}}{(k_{pm} - k_p)B_{pm}} \begin{Bmatrix} \tilde{\mathbf{U}}'_m \\ \tilde{\mathbf{W}}'_m \end{Bmatrix}, \tag{17}$$

$$\tilde{\mathbf{V}}' = \sum_{m=1}^{2M_a} \frac{(\phi_{aml}^L)^{\mathrm{T}}\tilde{\mathbf{F}}_{y'}}{(k_{am} - k_a)B_{am}} \tilde{\mathbf{V}}'_m, \tag{18}$$

where

$$B_{pm} = (\phi_{pmu}^L)^{\mathrm{T}}\phi_{pmu}^R - (\phi_{pml}^L)^{\mathrm{T}}\mathbf{K}_{p1}\phi_{pml}^R,$$
$$B_{am} = (\phi_{amu}^L)^{\mathrm{T}}\phi_{amu}^R - (\phi_{aml}^L)^{\mathrm{T}}\mathbf{K}_{a1}\phi_{aml}^R. \tag{19}$$

Moreover $(\tilde{\mathbf{U}}'_m\mathrm{T}, \tilde{\mathbf{W}}'_m\mathrm{T})^{\mathrm{T}} = \tilde{\mathbf{Q}}^R_{pm}$ and $\tilde{\mathbf{V}}'_m = \tilde{\mathbf{Q}}^R_{am}$ are the upper half of the eigenvectors corresponding to the eigenvalues k_{pm} and k_{am} for the plane-strain and anti-plane problems, respectively.

2.1.3. The Green function

A steady-state unit load is located, without loss of generality, at the origin of a plane, distance z_0 from the plate's top exterior surface, in order to construct the Green function. The spatial representation of this load, $\mathbf{f}(x, y)$, takes the form

$$\mathbf{f}(x, y) = \mathbf{f}_0\delta(x)\delta(y), \tag{20}$$

where

$$\mathbf{f}_0 = (f_x, f_y, f_z)^{\mathrm{T}} \tag{21}$$

represents the amplitude of the load in the x, y and z directions, respectively. Applying Fourier transform (4) to Eq. (20) gives the load, in the transformed domain, as

$$\tilde{\mathbf{f}} = \mathbf{f}_0. \tag{22}$$

Now $\tilde{\mathbf{f}}$ can be expressed in the (x', y', z) co-ordinate system as

$$\tilde{\mathbf{f}}' = \begin{Bmatrix} f_{x'} \\ f_{y'} \\ f_z \end{Bmatrix} = \begin{Bmatrix} f_x \cos\phi + f_y \sin\phi \\ -f_x \sin\phi + f_y \cos\phi \\ f_z \end{Bmatrix}. \tag{23}$$

Therefore, in the finite element formulation, the corresponding external nodal force vectors for the plane-strain and anti-plane problems, $\tilde{\mathbf{F}}_{x'z}$ and $\tilde{\mathbf{F}}_{y'}$, respectively, contain zero entries except at the load's nodal surface $z = z_0$. The (x', y', z) components in the plane-strain and anti-plane problems are $(f_{x'}, f_z)$ and $f_{y'}$, respectively, so that,

$$\tilde{\mathbf{F}}'_{x'z} = (0, \ldots, 0, f_{x'}, 0 \ldots, 0; 0, \ldots, 0, f_z, 0, \ldots, 0)^{\mathrm{T}}, \tag{24}$$

and

$$\tilde{\mathbf{F}}'_{y'} = (0, \ldots, 0, f_{y'}, 0 \ldots, 0)^{\mathrm{T}}. \tag{25}$$

2.1.3.1. Load in the z direction. In view of Eqs. (23)–(25) as well as Eqs. (17) and (18), a unit load in the z direction, $\tilde{\mathbf{f}}' = (0, 0, 1)^{\mathrm{T}}$, applied at $(0, 0, z_0)$ gives

$$(\phi^L_{pml})^{\mathrm{T}}\tilde{\mathbf{F}}'_{x'z} = \psi_{zp}, \quad (\phi^L_{aml})^{\mathrm{T}}\tilde{\mathbf{F}}'_{y'} = 0. \tag{26}$$

Here, ψ_{zp} corresponds to the element, ϕ^L_{pml}, for the plane-strain problem. It should be noted that, in this case, the displacements have no contribution from the anti-plane problem.

By means of Eqs. (17) and (18), the nodal displacement vector in the transformed domain can be written in the cylindrical co-ordinate system (r, θ, z) illustrated in Fig. 1 as

$$\begin{Bmatrix} \tilde{\mathbf{U}}_r \\ \tilde{\mathbf{U}}_\theta \\ \tilde{\mathbf{W}} \end{Bmatrix} = \sum_{m=1}^{2M_p} \frac{\psi_{zp}}{(k_{pm} - k_p)B_{pm}} \begin{Bmatrix} \tilde{\mathbf{U}}'_m \cos(\phi - \theta) \\ \tilde{\mathbf{U}}'_m \sin(\phi - \theta) \\ \tilde{\mathbf{W}}'_m \end{Bmatrix}. \tag{27}$$

Applying the inverse Fourier transform (5) to Eq. (27) gives the displacements in the spatial domain as [21]

$$\begin{aligned} \begin{Bmatrix} \mathbf{U}_r \\ \mathbf{U}_\theta \\ \mathbf{W} \end{Bmatrix} &= \frac{1}{(2\pi)^2} \int\int_{(k_p,\phi)} \begin{Bmatrix} \tilde{\mathbf{U}}_r \\ \tilde{\mathbf{U}}_\theta \\ \tilde{\mathbf{W}} \end{Bmatrix} e^{ik_p r \cos(\phi-\theta)} k_p \mathrm{d}k_p \, \mathrm{d}\phi \\ &= -\frac{1}{(2\pi)^2} \int\int_{(k_p,\phi)} \sum_{m=1}^{2M_p} \frac{\psi_{zp}}{B_{pm}} \left(1 + \frac{k_{pm}}{k_p - k_{pm}}\right) \begin{Bmatrix} \tilde{\mathbf{U}}'_m \cos(\phi - \theta) \\ \tilde{\mathbf{U}}'_m \sin(\phi - \theta) \\ \tilde{\mathbf{W}}'_m \end{Bmatrix} e^{ik_p r \cos(\phi-\theta)} \mathrm{d}k_p \, \mathrm{d}\phi. \end{aligned} \tag{28}$$

Zhu and Shah [13] demonstrated that only half the $2M_p$ modes associated with the waves propagating from the source towards the field points are relevant to the plane-strain problem. Therefore, by introducing $\varphi = \phi - \theta$, $(-\pi/2 \leqslant \varphi \leqslant \pi/2)$, Eq. (28) can be re-written as

$$\begin{Bmatrix} \mathbf{U}_r \\ \mathbf{U}_\theta \\ \mathbf{W} \end{Bmatrix} = -\frac{1}{(2\pi)^2} \int_{-\pi/2}^{\pi/2} \sum_{m=1}^{M_p} \frac{\psi_{zp}}{B_{pm}} \left(\int_{-\infty}^{\infty} e^{ik_p r \cos\varphi} \, \mathrm{d}k_p + \int_{-\infty}^{\infty} \frac{k_{pm}}{k_p - k_{pm}} e^{ik_p r \cos\varphi} \, \mathrm{d}k_p \right) \begin{Bmatrix} \tilde{\mathbf{U}}'_m \cos\varphi \\ \tilde{\mathbf{U}}'_m \sin\varphi \\ \tilde{\mathbf{W}}'_m \end{Bmatrix} \mathrm{d}\varphi. \tag{29}$$

By employing the definition of the Delta function,

$$\frac{1}{2\pi} \int_{-\infty}^{\infty} e^{ikr\cos\varphi} \mathrm{d}k = \delta(r \cos\varphi), \tag{30}$$

and applying Cauchy's residue theorem to the last integral in Eq. (29), it can be shown that

$$\begin{Bmatrix} \mathbf{U}_r \\ \mathbf{U}_\theta \\ \mathbf{W} \end{Bmatrix} = -\frac{1}{2\pi} \sum_{m=1}^{M_p} \frac{\psi_{zp}}{B_{pm}} \int_{-\pi/2}^{\pi/2} [\delta(r\cos\varphi) + ik_{pm} e^{ik_{pm} r \cos\varphi}] \begin{Bmatrix} \tilde{\mathbf{U}}'_m \cos\varphi \\ \tilde{\mathbf{U}}'_m \sin\varphi \\ \tilde{\mathbf{W}}'_m \end{Bmatrix} \mathrm{d}\varphi. \tag{31}$$

Note that the eigenvalues and associated eigenvectors affected by the isotropic material's properties (which are independent of ϕ) are incorporated in the derivation of Eq. (31).

By using the properties of the Delta function (see Hsu [22, appendix]), Eq. (31) can be simplified to

$$\left\{\begin{array}{c}\mathbf{U}_r\\ \mathbf{U}_\theta\\ \mathbf{W}\end{array}\right\}=\frac{1}{2}\sum_{m=1}^{M_p}\frac{\psi_{zp}}{B_{pm}}\left\{\begin{array}{c}k_{pm}\hat{H}_1(k_{pm}r)\tilde{\mathbf{U}}'_m\\ 0\\ [\frac{2}{\pi r}-\mathrm{i}k_{pm}\hat{H}_0(k_{pm}r)]\tilde{\mathbf{W}}'_m\end{array}\right\}. \tag{32}$$

It should be noted that the $\hat{H}_n$ in Eq. (32) are not Hankel functions. They take the form

$$\hat{H}_n(k_{pm}r)=\frac{\mathrm{e}^{-n\pi/2}}{\pi}\int_{-\pi/2}^{\pi/2}\mathrm{e}^{\mathrm{i}k_{pm}r\cos\varphi+in\varphi}\,\mathrm{d}\varphi. \tag{33}$$

2.1.3.2. Load in the x direction. As before, a unit load in the x direction, $\tilde{\mathbf{f}}'=(1,0,0)^{\mathrm{T}}$, is applied at $(0,0,z_0)$ so that

$$(\phi^L_{pml})^{\mathrm{T}}\tilde{\mathbf{F}}'_{x'z}=\psi_{xp}\cos\phi\ \text{ and }\ (\phi^L_{aml})^{\mathrm{T}}\tilde{\mathbf{F}}'_{y'}=-\psi_{xa}\sin\phi, \tag{34}$$

where ψ_{xp} and ψ_{xa} represent corresponding elements in the vectors ϕ^L_{pml} and ϕ^L_{aml} for the plane-strain and anti-plane problems, respectively.

In view of Eqs. (17) and (18), the nodal displacement vector in the transformed domain can be given in the cylindrical co-ordinate system (r,θ,z) as

$$\left\{\begin{array}{c}\tilde{\mathbf{U}}_r\\ \tilde{\mathbf{U}}_\theta\\ \tilde{\mathbf{W}}\end{array}\right\}=\sum_{m=1}^{2M_p}\frac{\psi_{xp}}{(k_{pm}-k_p)B_{pm}}\left\{\begin{array}{c}\tilde{\mathbf{U}}'_m\cos\phi\cos(\phi-\theta)\\ \tilde{\mathbf{U}}'_m\cos\phi\sin(\phi-\theta)\\ \tilde{\mathbf{W}}'_m\cos\phi\end{array}\right\}-\sum_{m=1}^{2M_a}\frac{\psi_{xa}}{(k_{am}-k_a)B_{am}}\left\{\begin{array}{c}-\tilde{\mathbf{V}}'_m\sin\phi\sin(\phi-\theta)\\ \tilde{\mathbf{V}}'_m\sin\phi\cos(\phi-\theta)\\ 0\end{array}\right\}. \tag{35}$$

Following the manipulations used to derive the Green function for a load in the z direction, the Green function due to a load in the x direction can be found similarly to be

$$\begin{aligned}\left\{\begin{array}{c}\mathbf{U}_r\\ \mathbf{U}_\theta\\ \mathbf{W}\end{array}\right\}=&-\frac{1}{2}\sum_{m=1}^{M_p}\frac{\psi_{xp}}{B_{pm}}\left\{\begin{array}{c}\frac{\mathrm{i}k_{pm}}{2}[\hat{H}_0(k_{pm}r)-\hat{H}_2(k_{pm}r)]\cos\theta\tilde{\mathbf{U}}'_m\\ \left\{\frac{2}{\pi r}\sin\theta-\frac{\mathrm{i}k_{pm}}{2}[\hat{H}_0(k_{pm}r)+\hat{H}_2(k_{pm}r)]\right\}\sin\theta\tilde{\mathbf{U}}'_m\\ k_{pm}\hat{H}_0(k_{pm}r)\cos\theta\tilde{\mathbf{W}}'_m\end{array}\right\}\\ &-\frac{1}{2}\sum_{m=1}^{M_p}\frac{\psi_{xa}}{B_{pm}}\left\{\begin{array}{c}\left\{-\frac{2}{\pi r}+\frac{\mathrm{i}k_{pm}}{2}[\hat{H}_0(k_{am}r)+\hat{H}_2(k_{am}r)]\right\}\sin\theta\tilde{\mathbf{V}}'_m\\ -\frac{\mathrm{i}k_{pm}}{2}[\hat{H}_0(k_{am}r)+\hat{H}_2(k_{am}r)]\sin\theta\tilde{\mathbf{V}}'_m\\ 0\end{array}\right\}.\end{aligned} \tag{36}$$

The Green function due to a load in the y direction, on the other hand, can be obtained by simply interchanging $\sin\theta$ and $\cos\theta$ and changing the sign of u_θ in Eq. (36).

2.2. Hybrid model for axisymmetric case

To check the previously formulated modal representation, a hybrid model (Zhu et al. [12]) is proposed for constructing the simpler axisymmetric Green function arising from a load in the z direction. Then the analytical formulation of the frequency equation and wave functions (Weaver and Pao [2]) is recast to study the outgoing, circular-crested waves travelling in a homogeneous isotropic plate. On the other hand, axisymmetric finite element modelling is employed in the vicinity of the point load. For the adopted cylindrical co-ordinate system (r, θ, z) shown in Fig. 1, the time-harmonic solutions to Eq. (1) can be expressed, for a homogeneous isotropic plate having no body forces, as

$$u_r = U(z')H_1^{(1)}(kr), \quad u_z = W(z')H_0^{(1)}(kr). \tag{37}$$

Here, $z' = z - H; k$ is the wave number and $H_0^{(1)}(kr)$, $H_1^{(1)}(kr)$ are Hankel functions of the first kind. The wave functions through the thickness are

$$U(z') = k(-B\sin\alpha z' + C\beta\sin\beta z') \text{ and } W(z') = \alpha B\cos\alpha z' + Ck^2\cos\beta z' \tag{38}$$

for the antisymmetric modes, and for the symmetric modes,

$$U(z') = -k(A\cos\alpha z' + D\,\beta\cos\beta z') \text{ and } W(z') = -\alpha A\sin\alpha z' + Dk^2\beta\sin\beta z', \tag{39}$$

with

$$\alpha^2 = \omega^2/c_p^2 - k^2, \quad \beta^2 = \omega^2/c_s^2 - k^2, \tag{40}$$

where c_p and c_s are the longitudinal and shear wave speeds, respectively.

For a homogeneous plate, the amplitude relations and frequency equations can be obtained by satisfying the traction free conditions on the exterior surfaces of the plate. Consequently

$$\frac{B}{C} = \frac{2\beta k^2\sin\beta H}{(k^2-\beta^2)\sin\alpha H}, \quad \frac{A}{D} = \frac{-2\beta k^2\cos\beta H}{(k^2-\beta^2)\cos\alpha H}, \tag{41}$$

$$(k^2-\beta^2)\sin\alpha H\cos\beta H + 4\alpha\beta k^2\cos\alpha H\sin\beta H = 0, \tag{42}$$

for the antisymmetric modes, and

$$(k^2-\beta^2)\cos\alpha H\sin\beta H + 4\alpha\beta k^2\sin\alpha H\cos\beta H = 0, \tag{43}$$

for the symmetric modes. Eqs. (42) and (43) are identical to the Rayleigh–Lamb frequency equations for straight-crested waves that occur under plane-strain conditions. For a given ω, these two equations serve as implicit transcendental functions of k whose solutions give the wave numbers. The corresponding wave functions can be computed from Eqs. (38) and (39). Propagator matrices are used to construct the wave modes described by Zhu et al. [12] for a layered plate.

A hybrid method is employed to compute the axisymmetric Green function of an isotropic plate as well as a layered plate due to a vertical point load applied at $(0, 0, z_0)$. Then the plate is divided into exterior and interior regions by using a cylindrical surface having radius r_0, as illustrated in Fig. 2. Formulations appropriate to each of these regions are detailed next.

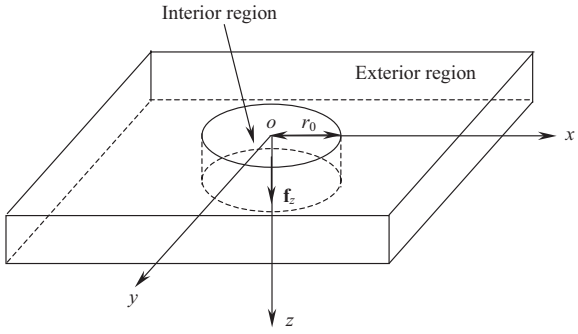

Fig. 2. The interior and exterior regions.

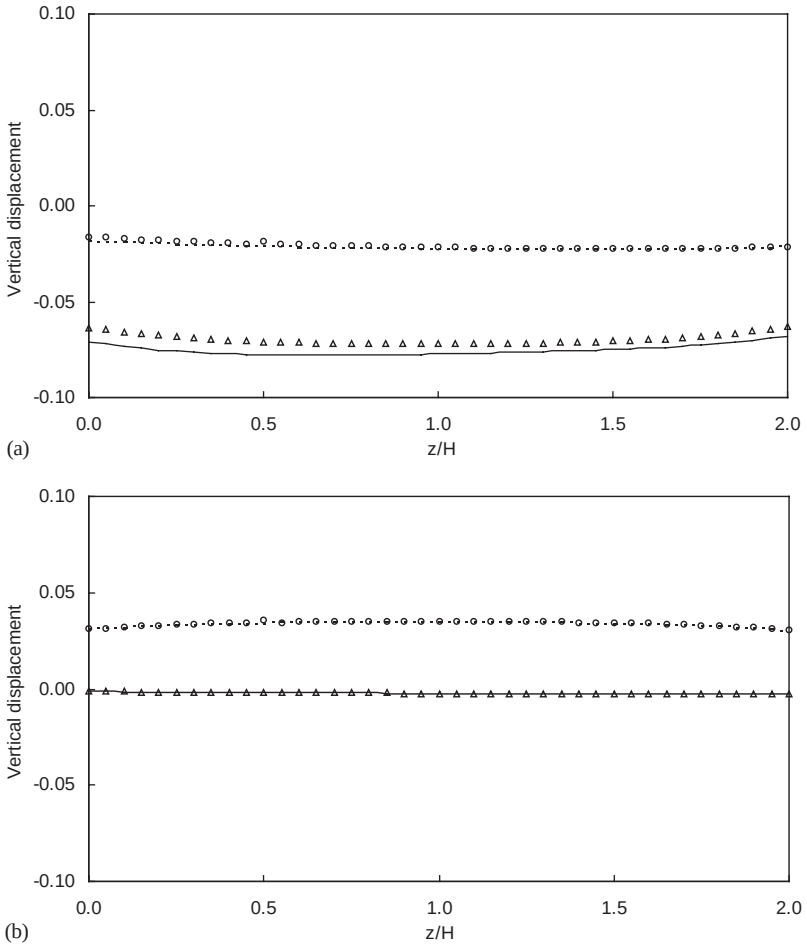

Fig. 3. Vertical load induced vertical displacements for a homogeneous plate when $\Omega = 1$: (a) $x = 2H$, and (b) $x = 10H$ (—, $Re(w)$ from hybrid method; - - - -, $Im(w)$ from hybrid method; Δ, $Re(w)$ from superposition method; o, $Im(w)$ from superposition method).

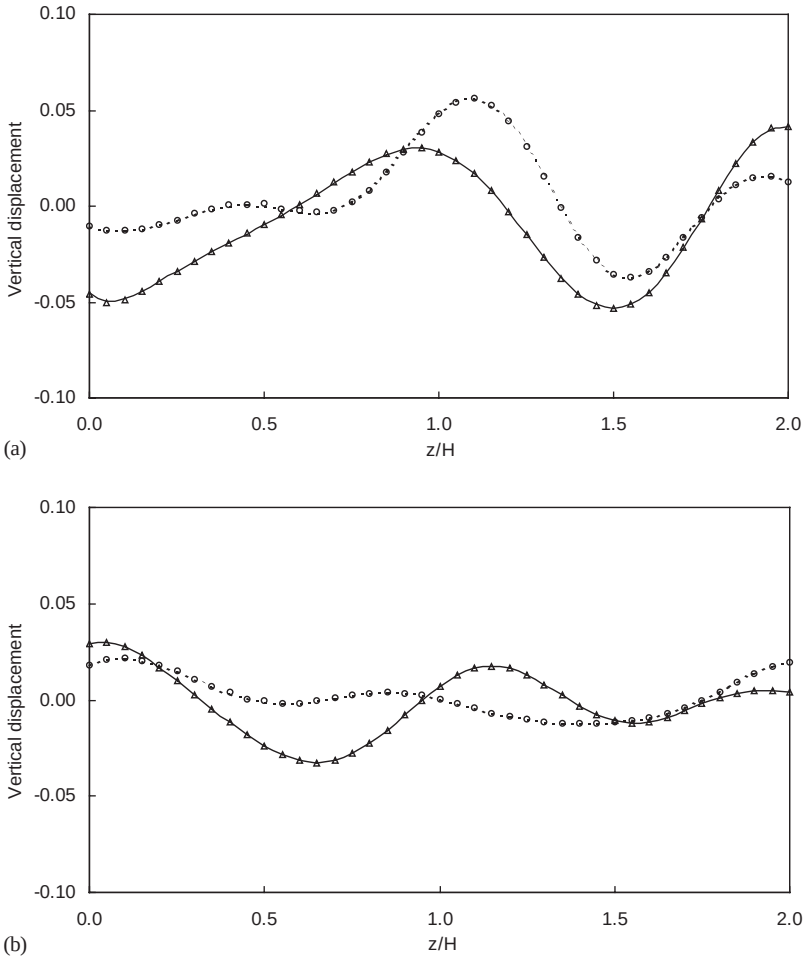

Fig. 4. Vertical load induced vertical displacements for a homogeneous plate when $\Omega = 10$: (a) $x = 2H$, (b) $x = 10H$ (—, $Re(w)$ from hybrid method; - - - -, $Im(w)$ from hybrid method; Δ, $Re(w)$ from superposition method; o, $Im(w)$ from superposition method).

2.2.1. *Wave function expansion in the exterior region*

The plate is divided into N sublayers in the exterior region in order to evaluate the wave functions given by Eqs. (38) and (39). The displacement field is represented by a modal summation involving a finite number ($M_p = 2(2N + 1)$) of modes in the form

$$\mathbf{U}_r = \sum_{m=1}^{M_p} A_m \mathbf{U}_m H_1^{(1)}(k_m r), \quad \mathbf{U}_z = \sum_{m=1}^{M_p} A_m \mathbf{W}_m H_0^{(1)}(k_m r), \tag{44}$$

where $(\mathbf{U}_m^{\mathrm{T}}, \mathbf{W}_m^{\mathrm{T}})^{\mathrm{T}}$ is the mth right eigenvector corresponding to eigenvalue k_m, A_m is the amplitude of the mth mode that is to be determined. Eq. (44) gives the displacements at the

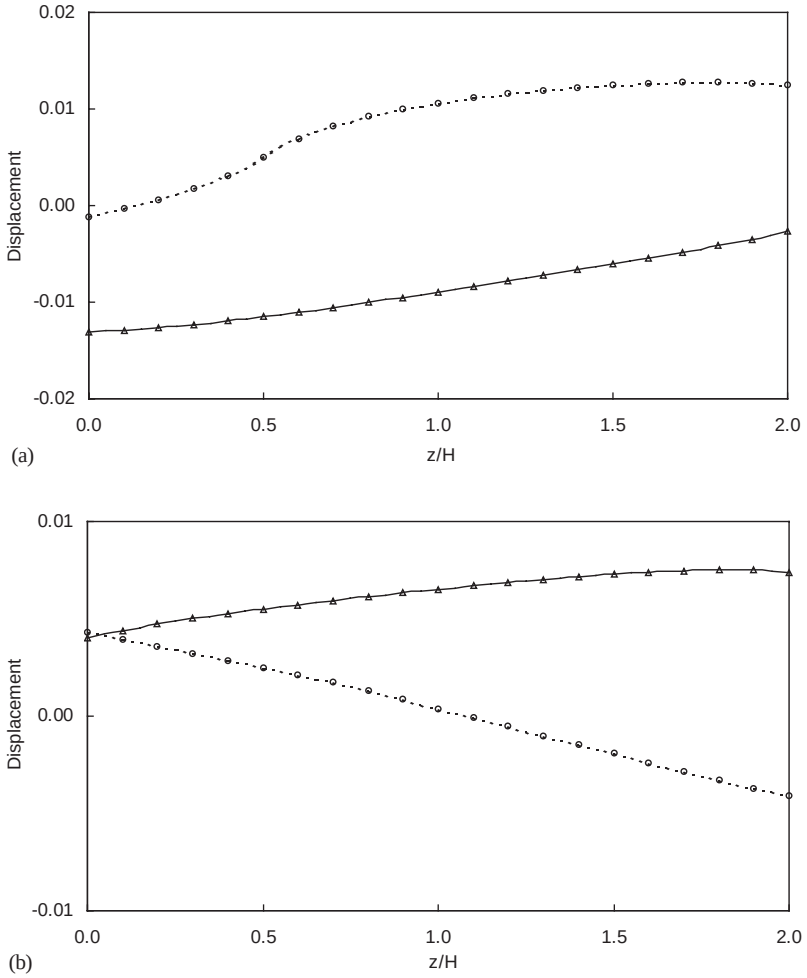

Fig. 5. Reciprocity check for a homogeneous plate's displacement when $\Omega = 1$: (a) $x = 2H$, (b) $x = 10H$ (——, $Re(w)$ due to a horizontal load; - - - -, $Im(w)$ due to a horizontal load; Δ, $Re(w)$ due to a vertical load; o, $Im(w)$ due to a vertical load).

boundary nodes as

$$\mathbf{q}_B = \boldsymbol{G}\Lambda, \tag{45}$$

where subscript B denotes the boundary between the interior and exterior regions and

$$\boldsymbol{G} = \begin{bmatrix} \mathbf{U}_1 H_1^{(1)}(k_1 r_0), \ldots, \mathbf{U}_m H_1^{(1)}(k_m r_0), \ldots, \mathbf{U}_{M_p} H_1^{(1)}(k_{M_p} r_0) \\ \mathbf{W}_1 H_0^{(1)}(k_1 r_0), \ldots, \mathbf{W}_m H_0^{(1)}(k_m r_0), \ldots, \mathbf{W}_{M_p} H_0^{(1)}(k_{M_p} r_0) \end{bmatrix}, \tag{46}$$

with

$$\Lambda = (A_1, \ldots, A_m, \ldots, A_{M_p})^{\mathrm{T}}. \tag{47}$$

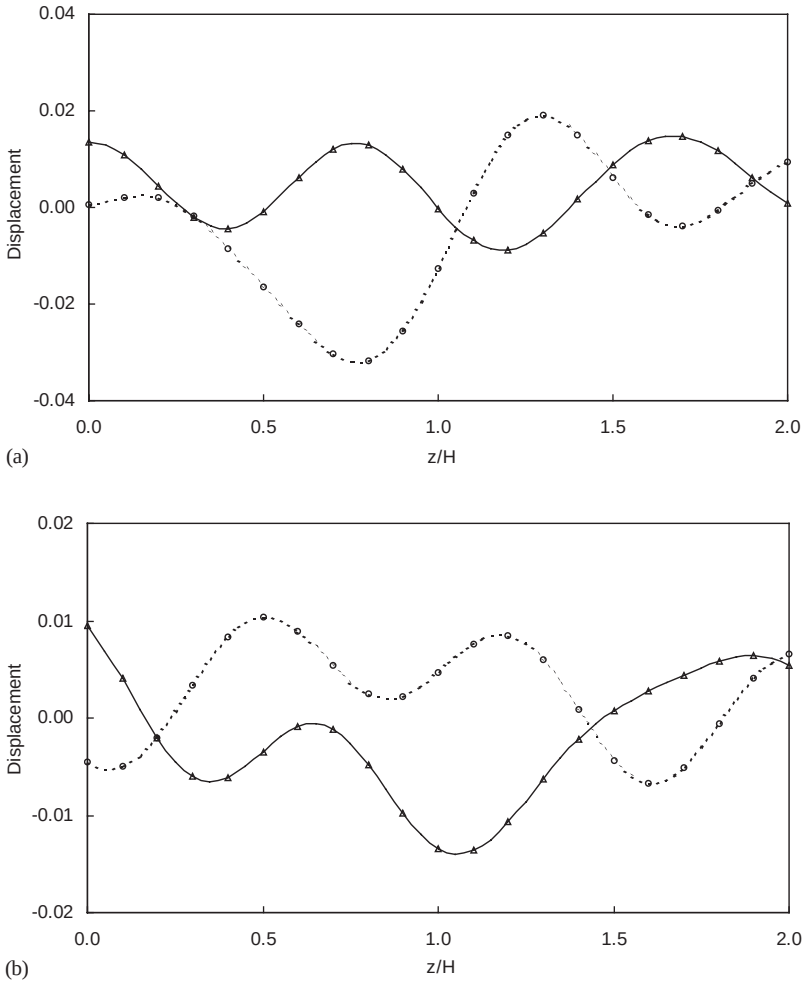

Fig. 6. Reciprocity check for a homogeneous plate's displacement when $\Omega = 10$: (a) $x = 2H$, (b) $x = 10H$ (——, $Re(w)$ due to a horizontal load; - - - -, $Im(w)$ due to a horizontal load; Δ, $Re(w)$ due to a vertical load; o, $Im(w)$ due to a vertical load).

Here, r_0 is the radial boundary between the interior and exterior regions. The nodal force vector at the boundary nodes can be formed as

$$P_B = \mathbf{F}\Lambda, \tag{48}$$

where

$$\mathbf{F} = \begin{bmatrix} \mathbf{f}_{r1}, \ldots, \mathbf{f}_{rm}, \ldots, \mathbf{f}_{rM_p} \\ \mathbf{f}_{z1}, \ldots, \mathbf{f}_{zm}, \ldots, \mathbf{f}_{zM_p} \end{bmatrix}. \tag{49}$$

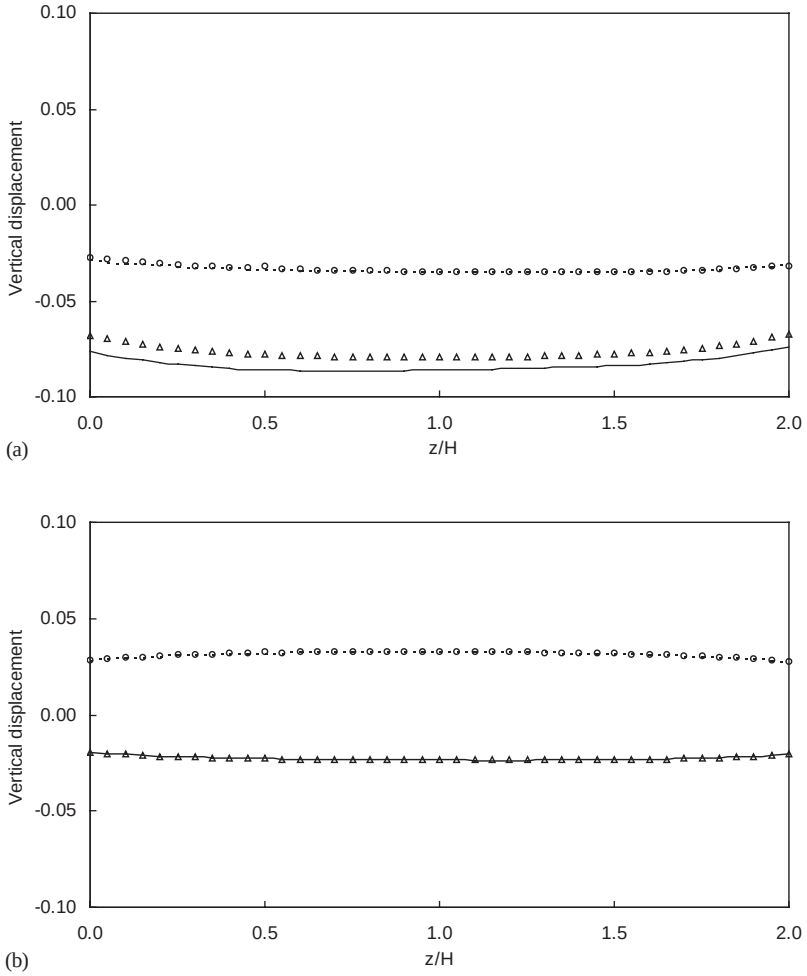

Fig. 7. Vertical load induced vertical displacements for a 3-ply laminated plate when $\Omega = 1$: (a) $x = 2H$, (b) $x = 10H$ (—, $Re(w)$ from hybrid method; - - - -, $Im(w)$ from hybrid method; Δ, $Re(w)$ from superposition method; o, $Im(w)$ from superposition method).

The $\mathbf{f}_{rm}$ and $\mathbf{f}_{zm}$ are generated here by using a consistent load vector formulation. Subscripts r and z denote the direction of the evaluated force mode vectors.

2.2.2. *Finite element model of interior region*

The interior region is modelled by employing axisymmetric finite elements. By following the conventional process of assembling finite elements [23], the minimal energy functional of the system's governing equations can be obtained from

$$\delta\hat{\pi} = \delta\bar{\mathbf{q}}_T^{\mathrm{T}}\mathbf{S}\mathbf{q}_T - \delta\bar{\mathbf{q}}_T^{\mathrm{T}}\mathbf{P}_T = 0, \tag{50}$$

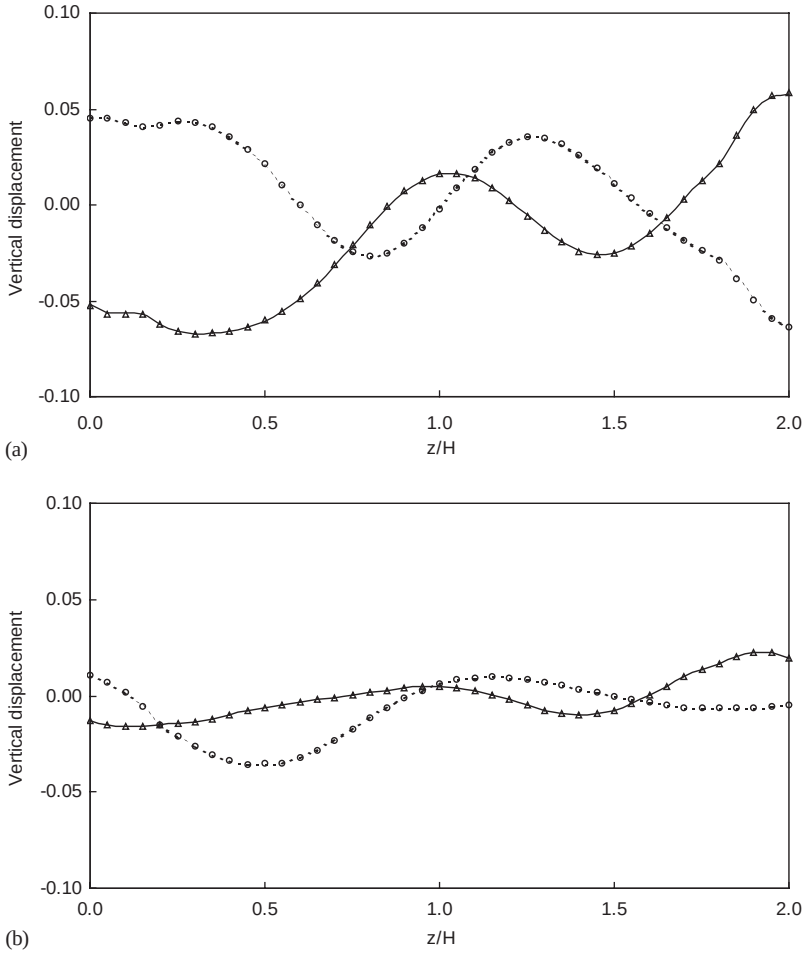

Fig. 8. Vertical load induced vertical displacements for a 3-ply laminated plate when $\Omega = 10$: (a) $x = 2H$, (b) $x = 10H$ (——, $Re(w)$ from hybrid method; - - - -, $Im(w)$ from hybrid method; Δ, $Re(w)$ from superposition method; o, $Im(w)$ from superposition method).

where

$$\mathbf{q}_T = \begin{Bmatrix} \mathbf{q}_I \\ \mathbf{q}_B \end{Bmatrix}, \quad \mathbf{P}_T = \begin{Bmatrix} \mathbf{P}_I \\ \mathbf{P}_B \end{Bmatrix}, \quad \mathbf{S} = \mathbf{K}_T - \omega^2 \mathbf{M}_T = \begin{bmatrix} \mathbf{S}_{II} & \mathbf{S}_{IB} \\ \mathbf{S}_{BI} & \mathbf{S}_{BB} \end{bmatrix}, \tag{51}$$

and an over bar denotes the conjugate of a complex matrix. In Eq. (51), $\mathbf{q}_I$ and $\mathbf{P}_I$ are the nodal displacement and force vectors corresponding to the interior nodes whereas $\mathbf{q}_B$ and $\mathbf{P}_B$ correspond to the boundary nodes. $\mathbf{K}_T$ and $\mathbf{M}_T$ are the global stiffness and mass matrices of the interior region, respectively.

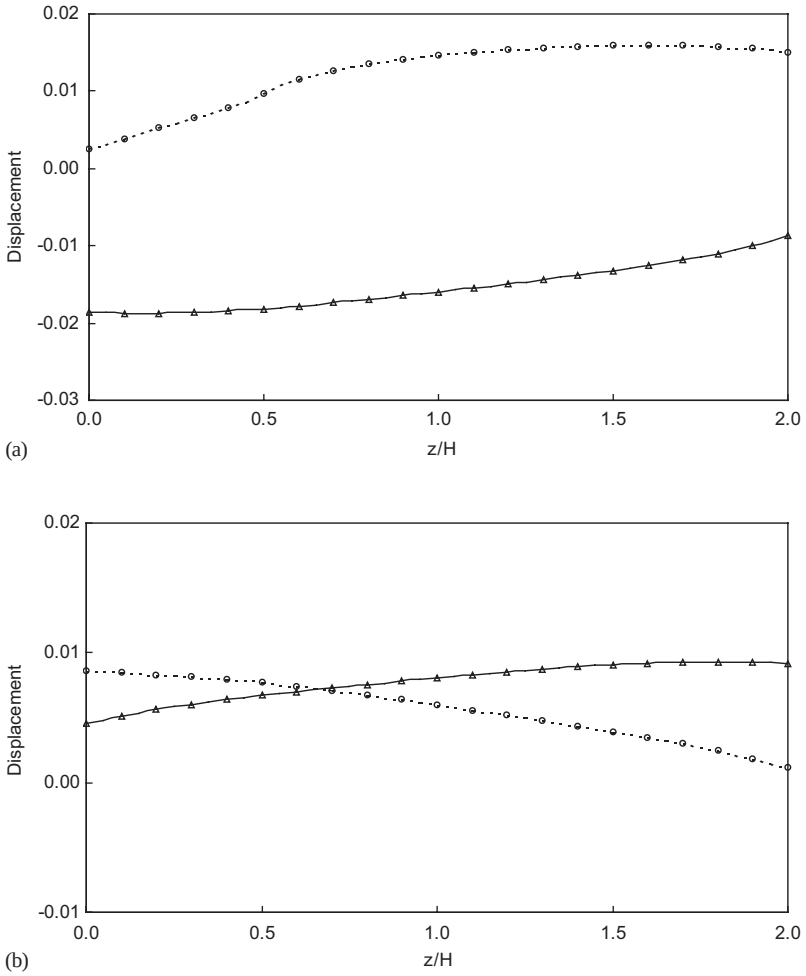

Fig. 9. Reciprocity check for a 3-ply laminated plate's displacement when $\Omega = 1$: (a) $x = 2H$, (b) $x = 10H$ (—, $Re(w)$ due to a horizontal load; - - - -, $Im(w)$ due to a horizontal load; Δ, $Re(w)$ due to a vertical load; o, $Im(w)$ due to a vertical load).

2.2.3. Global solution

By imposing continuity conditions for the displacements and tractions on the boundary nodes, a system of linear algebraic equations can be obtained for the global solution as

$$\bar{\mathbf{G}}^{\mathrm{T}}(\mathbf{S}^{*}_{BB}\mathbf{G} - \mathbf{F})\Lambda = -\bar{\mathbf{G}}^{\mathrm{T}}\mathbf{S}_{BI}\mathbf{S}_{II}^{-1}\mathbf{P}_{I}, \tag{52}$$

where

$$\mathbf{S}^{*}_{BB} = \mathbf{S}_{BB} - \mathbf{S}_{BI}\mathbf{S}_{II}^{-1}\mathbf{S}_{IB}. \tag{53}$$

Once the A_m are evaluated, the axisymmetric Green function can be found by using Eq. (44).

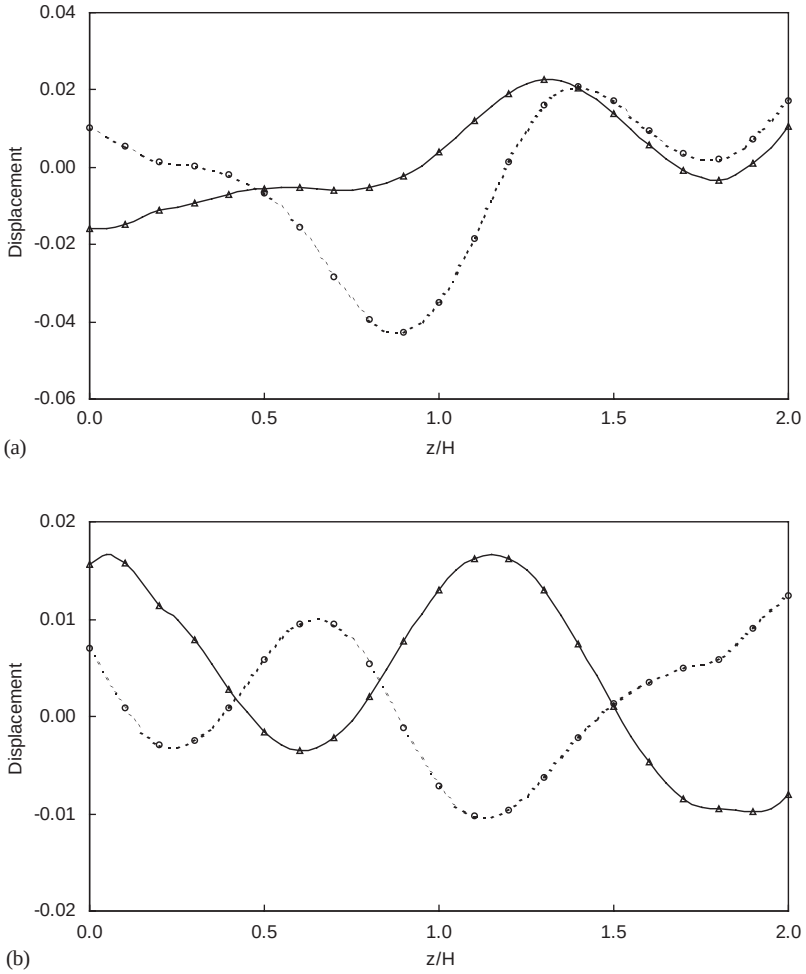

Fig. 10. Reciprocity check for a 3-ply laminated plate's displacement when $\Omega = 10$: (a) $x = 2H$, (b) $x = 10H$ (——, $Re(w)$ due to a horizontal load; - - - -, $Im(w)$ due to a horizontal load; Δ, $Re(w)$ due to a vertical load; o, $Im(w)$ due to a vertical load).

3. Numerical results and discussion

Numerical examples are presented in this section for the displacement Green functions of a homogeneous isotropic plate as well as a layered plate.

Example 1. A homogeneous isotropic plate with the Poisson ratio $v = 1/3$ is considered. The normalized shear modulus μ is taken as 1.

Example 2. A 3-ply laminated plate is investigated. It is symmetric about the middle plane. Layers 1 and 3 are at the top ($z = 0$) and bottom ($z = 2H$) of the plate, respectively, with layer 2 in the

middle. The outer layers are assumed to be aluminum that sandwich the middle steel layer. The material constants and geometric data are given by the Poisson ratio, v, shear modulus, μ, mass density, ρ, and laminate thicknesses, H. They are taken as

$$v_2 = 0.28, \mu_2 = 75 \times 10^9\ \mathrm{N/m^2}, \rho_2 = 7.8 \times 10^3\ \mathrm{kg/m^3}, H_2 = 1.6H,$$

$$v_1 = v_3 = 0.32, \mu_1 = \mu_3 = 25 \times 10^9\ \mathrm{N/m^2}, \rho_1 = \rho_3 = 2.7 \times 10^3\ \mathrm{kg/m^3}, H_1 = H_3 = 0.2H,$$

where a subscript denotes the corresponding layer. In the numerical results the material constants μ_i and $\rho_i (i = 1, 2, 3)$ are normalized by those of the middle layer, respectively.

The normalized frequency $\Omega = \omega H/\sqrt{\mu/\rho}$ is used for Example 1. It is replaced by $\Omega = \omega H/\sqrt{\mu_2/\rho_2}$ for Example 2. The displacements for both the examples are normalized with respect to H. Two loads are considered for both plates. One corresponds to a vertical load, the other to a horizontal load in the x direction. These loads act separately at the same location (0, 0, 0.5 H). Axisymmetry about the z-axis holds for the vertical load but not for the horizontal load. Therefore, the hybrid method, presented here, can be used for the former but not for the latter situation. However, the plane-wave superposition technique is applicable to both loads. In the hybrid model, the finite element mesh contains 20 quadratic elements and 85 nodes. The boundary is located at $r_0 = 0.2H$, as shown in Fig. 2. Forty modes are employed in the wave function expansion in the exterior region.

Results are given in Figs. 3–6 for Example 1. Fig. 3(a) and (b) compare the vertical displacement (w) computed through the thickness at sections $x = 2H$ and $x = 10H$ for a frequency $\Omega = 1$. The corresponding results are presented in Fig. 4 for $\Omega = 10$. Both the hybrid method as well as the plane-wave superposition techniques are used in Figs. 3 and 4. Here, $Re(w)$ and $Im(w)$ refer to the real and imaginary part of a complex displacement, respectively. $Re(w)$ and $Im(w)$ are almost constant through the thickness in Fig. 3 when $\Omega = 1$. However, when Ω is increased to ten, they oscillate noticeably through the thickness as seen in Fig. 4. Both Figs. 3 and 4 show that the data from the two approaches agree well, especially when $x = 10H$ (i.e., in the far field).

Figs. 5 and 6 present the vertical displacement distribution through the thicknesses at $x = 2H$ and $10H$ when a horizontal x direction load acts at (0, 0, 0.5H). Figs. 5 and 6 correspond to $\Omega = 1$ and 10, respectively. The dynamic reciprocal identity (Betti–Rayleigh Theorem [24]) is used to check the validity of the results. For example, in Fig. 5(a) the solid (—) and dashed (- - - -) curves indicate the vertical displacement through the thickness at $x = 2H$ when a horizontal load acts at (0,0,0.5H). The distribution was evaluated by using Eq. (36). The same results are recovered by applying a vertical load at ($2H$,0,z_0) where z_0 coincides with one of the $(2N + 1)$ node points. The results, shown by circles (o) and triangles (Δ) in the figure, are calculated with the aid of Eq. (32). Similar results are presented in Figs. 5(b), 6(a) and (b). From these figures it can be inferred that satisfaction of the reciprocity relations confirms the correctness of the proposed superposition algorithm. As observed earlier, the results for $\Omega = 10$ exhibit an oscillatory behavior.

To demonstrate the versatility of the plane-wave superposition method, the results for the 3-ply laminated plate of Example 2 are given in Fig. 7–11. The overall behavior of the displacement distribution is shown to be similar to that of the homogeneous plate considered in Example 1.

Fig. 11 shows the vertical displacement's variation along the top surface ($z = 0$) of the plate due to a vertical point load. Since $r = 0$ is a singular point of the solution, the results presented here

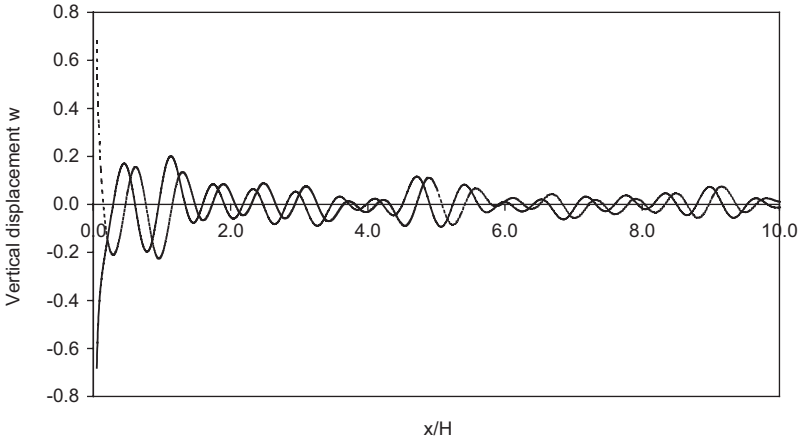

Fig. 11. Vertical displacement distribution along top surface ($z = 0$) of a 3-ply laminated plate due to a vertical load when $\Omega = 10$; ——, $Re(w)$; - - -, $Im(w)$.

apply only for $0.05H \leqslant r \leqslant 10H$. A detailed study near $r = 0$ shows a noticeable jump in the vertical displacement but these results are not shown for brevity.

4. Conclusions

A plane-wave superposition method is used to compute the three dimensional, steady state Green function for a laminated plate. It is validated for a vertical load by the invariably close agreement with independently obtained results from a hybrid finite element method. Such a validation is not possible with the hybrid modelling presented here for a horizontal load. However, it is feasible to check the displacement reciprocity relation which is satisfied. Moreover, the general displacement behavior of the homogeneous and laminated plates considered is shown to be similar.

Acknowledgements

The work presented in this paper is supported by the Natural Science and Engineering Research Council of Canada (grant OGP007988).

References

[1] J. Miklowitz, The Theory of Elastic Waves and Waveguides, North-Holland, Amsterdam, 1978.
[2] R.L. Weaver, Y.H. Pao, Axisymmetric waves excited by a point source in a plate, American Society of Mechanical Engineers Journal of Applied Mechanics 49 (1982) 821–836.
[3] A.N. Ceranoglu, Y.H. Pao, Propagation of elastic pulse and acoustic emission in a plate, American Society of Mechanical Engineers Journal of Applied Mechanics 48 (1981) 125–147.

[4] N. Vasudevan, A.K. Mal, Response of an elastic plate to localized transient sources, American Society of Mechanical Engineers Journal of Applied Mechanics 52 (1985) 356–362.
[5] R.A. Scott, J. Miklowitz, Transient elastic waves in anisotropic plates, American Society of Mechanical Engineers Journal of Applied Mechanics 34 (1) (1967) 104–110.
[6] R.A. Scott, J. Miklowitz, Near-field transient waves in anisotropic elastic plates for two and three dimensional problems, International Journal of Solids and Structures 5 (10) (1969) 1059–1075.
[7] J.R. Willis, R.J. Bedding, Transient elastodynamic fields in anisotropic plates and layers, in: J. Miklowitz, J.D. Achenbach (Eds.), Modern Problems in Elastic Wave Propagation, Wiley Interscience, New York, 1978, pp. 347–371.
[8] W.A. Green, E.R. Green, Penetration of impact stresses in laminated composite plates, in: A.K. Mal, Y.D.S. Rajapakse (Eds.), Impact Response and Elastodynamics of Composites, AMD-Vol. 116, ASME, New York, 1990, pp. 135–152.
[9] E.R. Green, Transient impact response of a fiber composite laminate, Acta Mechanica 86 (1-4) (1991) 153–165.
[10] E.R. Green, The effect of different impact time histories on the response of a fiber composite plate, in: L. Schwer, J.N. Reddy, A. Mal (Eds.), Enhancing Analysis Techniques for Composite Materials, NDE-Vol.10, ASME, New York, 1991, pp. 9–21.
[11] G.R. Liu, J. Tani, T. Ohyoshi, K. Watanabe, Transient waves in anisotropic laminated plate, part I: theory; part II: application, American Society of Mechanical Engineers Journal of Vibration and Acoustics 113 (1991) 230–239.
[12] J. Zhu, A.H. Shah, S.K. Datta, Modal representation of two-dimensional elastodynamic green's functions, American Society of Civil Engineers Journal of Engineering Mechanics 121 (1) (1995) 26–36.
[13] J. Zhu, A.H. Shah, A hybrid method for transient wave scattering by flaws in composite plates, International Journal of Solids and Structures 34 (14) (1997) 1719–1734.
[14] R.L. Weaver, W. Sachse, K.Y. Kim, Transient elastic waves in a transversely isotropic plate, American Society of Mechanical Engineers Journal of Applied Mechanics 63 (1996) 337–345.
[15] A.K. Mal, S.S. Lih, Elastodynamic response of a unidirectional composite laminate to concentrated surface loads: part I, American Society of Mechanical Engineers Journal of Applied Mechanics 59 (1992) 878–886.
[16] P.C. Xu, A.K. Mal, An adaptive integration scheme for irregularly oscillatory functions, Wave Motion 7 (1985) 235–243.
[17] P.C. Xu, A.K. Mal, Calculation of the green's functions for a layered viscoelastic solid, Bulletin of the Seismological Society of America 77 (1987) 1823–1837.
[18] S.B. Dong, K.H. Huang, Edge vibrations in laminated composite plates, American Society of Mechanical Engineers Journal of Applied Mechanics 52 (2) (1985) 433–438.
[19] J. Zhu, A.H. Shah, S.K. Datta, Transient response of a composite plate with delamination, American Society of Mechanical Engineers Journal of Applied Mechanics 65 (1998) 664–670.
[20] G.R. Liu, J.D. Achenbach, Strip element method to analyze wave scattering by cracks in anisotropic laminated plates, American Society of Mechanical Engineers Journal of Applied Mechanics 62 (1995) 607–613.
[21] J.A. Stratton, Electromagnetic Theory, McGraw-Hill, New York, 1941.
[22] H.P. Hsu, Fourier Analysis, Simon and Schuster, New York, 1972.
[23] K.J. Bathe, Finite Element Procedures in Engineering Analysis, Prentice-Hall, Englewood Cliffs, NJ, 1982.
[24] J.D. Achenbach, Wave Propagation in Solids, Elsevier, New York, 1975.